FINAL REPORT
ON
NASA AMES RESEARCH CENTER
COOPERATIVE AGREEMENT
NCC2-955

Title:

Atmospheric Dynamics on Venus, Jupiter, and Saturn: An Observational and Analytical Study

Period of Agreement:
July 1, 1996 – April 30, 2000

Date of Report:
May 31, 2000

Principal Investigator:
Professor Alison Bridger
Department of Meteorology
San Jose State University
One Washington Square
San Jose, CA 95192-0104
(408) 924-5206
e-mail: bridger@hellas.arc.nasa.gov

Co-Investigators:
Dr. Julio A. Magalhães
(San Jose State University Foundation)
Research Associate
Space Science Division
NASA-Ames Research Center, Mail Stop 245-3
Moffett Field, CA 94035-1000
(415) 604-3116 / FAX: (415) 604-6779
e-mail: jmagalhaes@mail.arc.nasa.gov

Dr. Richard E. Young
Research Scientist
Space Science Division
NASA-Ames Research Center, Mail Stop 245-3
Moffett Field, CA 94035-1000
(415) 604-5521 / FAX: (415) 604-6779
e-mail: reyoung@mail.arc.nasa.gov

Stratification of Jupiter's troposphere at the Galileo Probe Entry Site

Determining the static stability of Jupiter's atmosphere below the visible cloud levels is important for understanding the dynamical modes by which energy and momentum are transported through Jupiter's deep troposphere. The Galileo Probe Atmospheric Structure Investigation (ASI) employed pressure and temperature sensors to directly measure these state variables during the parachute-descent phase, which started at a pressure (p) of 0.4 bars and ended at p= 22 bars. The internal temperature of the probe underwent large temperature fluctuations which significantly exceeded design specifications. Corrections for these anomalous interior temperatures have been evaluated based on laboratory data acquired after the mission using the flight spare hardware. The corrections to the pressure sensor readings was particularly large and the uncertainties in the atmospheric pressures derived from the p sensor measurements may still be significant. We have sought to estimate the formal uncertainties in the static stability derived from the p and T sensor measurements directly and to devise means of assessing the static stability of Jupiter's atmosphere which do not rely on the p sensor data.

Figure 1 presents the background static stability derived directly from the p and T sensor data with three assumptions for the para-H_2 fraction. The background lapse rate used for the static stability has been derived by filtering p and T using a standard digital filter which passes only spatial frequencies with vertical wavelengths greater $\geq$ 50 km. Since the the NMS experiment indicates water and ammonia are sub-saturated, the static stabilities are based on the dry adiabat. c_p for H_2 is computed from the routine of Smith and Gierasch (1995), which has been verified over the full p and T range of the Galileo Probe descent by comparison to experimental data. The three solid curves represent three assumptions for the para-H_2 fraction (f_p): an equilibrium adiabat, the so-called normal (high T) adiabat, and an adiabat based on the value measured for the upper troposphere by Voyager IRIS at the latitude of the Galileo Probe Probe Entry Site (PES). c_p for He, CH_4, NH_3, and H_20 are based on experimental data corresponding to the conditions encountered by the probe. Abundances are obtained from Niemann et al (1998) and Folkner et al (1998). The dotted lines represent the formal uncertainties in the static stability for the dry adiabat. The listed uncertainties are based on treating the errors in p and T presented in Seiff et al (1998) as following a Gaussian distribution. Uncertainties in g and the molecular abundances are also included in the evaluation of the uncertainties in the static stability (~1% effect).

Since the T sensor data was essentially unaffected by the thermal anomaly in the probe, we have derived an approach for evaluating the background lapse rate of the atmosphere using only data from the T sensor. For a probe in equilibrium descent (drag force= gravity) traveling through an ideal gas atmosphere in hydrostatic balance with a constant lapse rate, the following expression for the variation of the measured T with time can be found:

$$T(t) = T_O[a(t-t_O) + 1]^b \qquad (1)$$

where

$$a = \frac{\left[\frac{g}{RdT/dz} - 1\right]}{2T_0/\,dT/dz}\left(\frac{2mg}{C_D A \rho_0}\right)^{1/2}, \qquad b = \frac{-2}{\left[\frac{g}{RdT/dz} - 1\right]}$$

dT/dz is the lapse rate; T_0 and ρ_0 are temperature and density at time t_0, respectively; m/C_DA is the ballistic coefficient of the parachute; g and R are the acceleration of gravity and gas constant, respectively. This expression assumes m/C_DA, g , and R are constant over the interval of the fit; vertical wind is also assumed to be small compared to the probe's descent velocity (w> 30 m/s).

Figure 1:

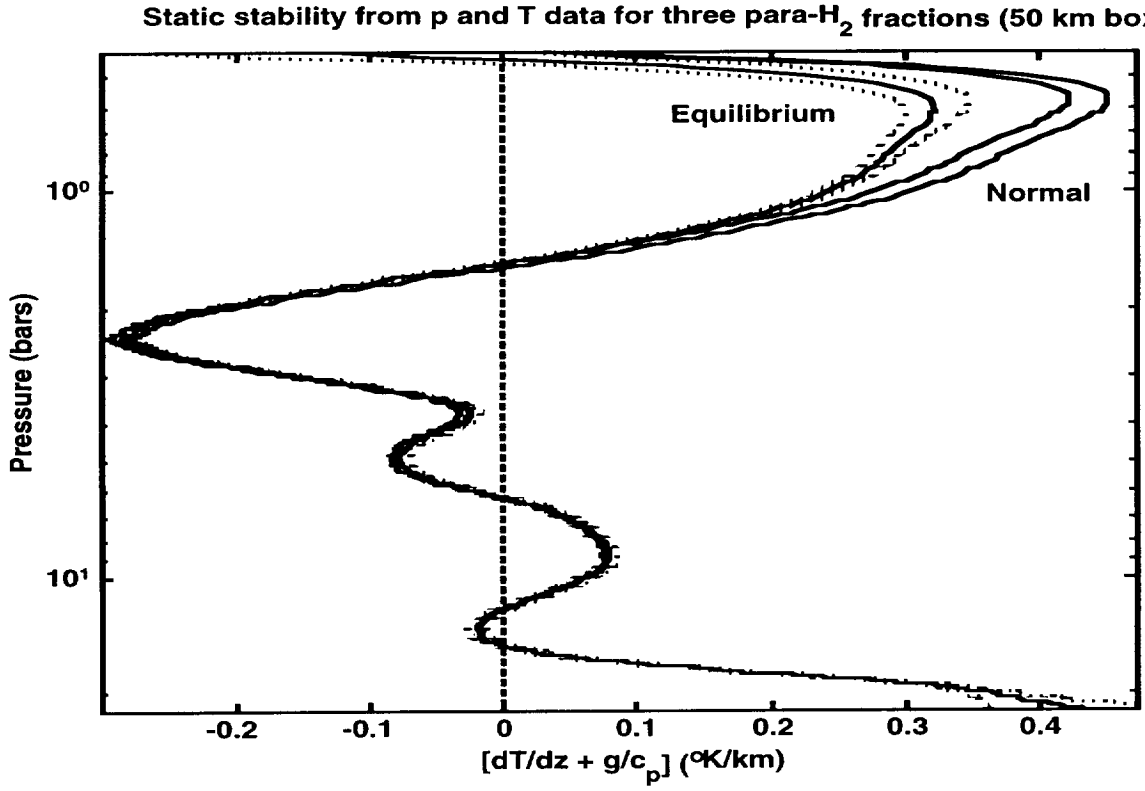

Our approach to evaluating the lapse rate is to fit the T sensor data over some altitude interval to eq. (1), and to then derive the lapse rate from the coefficient b using known g and R. We "march" eq. (1) through the data set by including all points within a box of some specified width about each observation. This procedure is analogous to the procedure used to define the background lapse rate from p and T described above. Note that our approach allows for slowly varying g, R, and m/C_DA. Since we are interested in the mean large scale ("background") lapse rate, the assumption of a constant lapse rate within each marching box, is appropriate. We have also investigated the effects of small deviations from equilibrium descent using a perturbation approach based on the zeroth order solution provided by eq. (1). Effects of the correction are small as would be expected based on the short timescale (~10 s) for the achievement of equilibrium descent, which is confirmed by the measured accelerations being within 1% of g soon after the start of the parachute descent phase.

Figure 2a presents the static stability derived from fits to eq. (1) with a 50 km marching box and and the previously discussed three assumptions for f_p for the calculation of c_p. Note the broad region of static stability (0.1-0.2 K/km) between p~ 0.6 bars down to p~10 bars. Note that narrow regions of static instability exist near p~ 0.5 bars and p~10 bars; the region at p~ 0.5 bars is likely due to an edge effect from the filtering procedure. For comparison the static stability derived from the p and T data is displayed as a dashed line. The static stability we have derived from T alone appears to be more physically reasonable than that derived from p and T since the latter displays broad regions of static instability, which are physically unrealistic due to the rapid vertical tranport of heat implied by the strong buoyancy accelerations associated with the static instability . As discussed further below, the observed vertical gradients in molecular weight at p< 5 bars are too low to stabilize the regions of static instability derived using p and T. In addition, note that the magnitude of the static stability derived from T alone is consistent with the values required by a linear equatorially-trapped Rossby wave interpretation of the 5-micron hot spots (Ortiz et al, 1998) and from a study of mesoscale wave packets observed by Voyager (cf. Flasar and Gierasch, 1986).

Figure 2a, b:

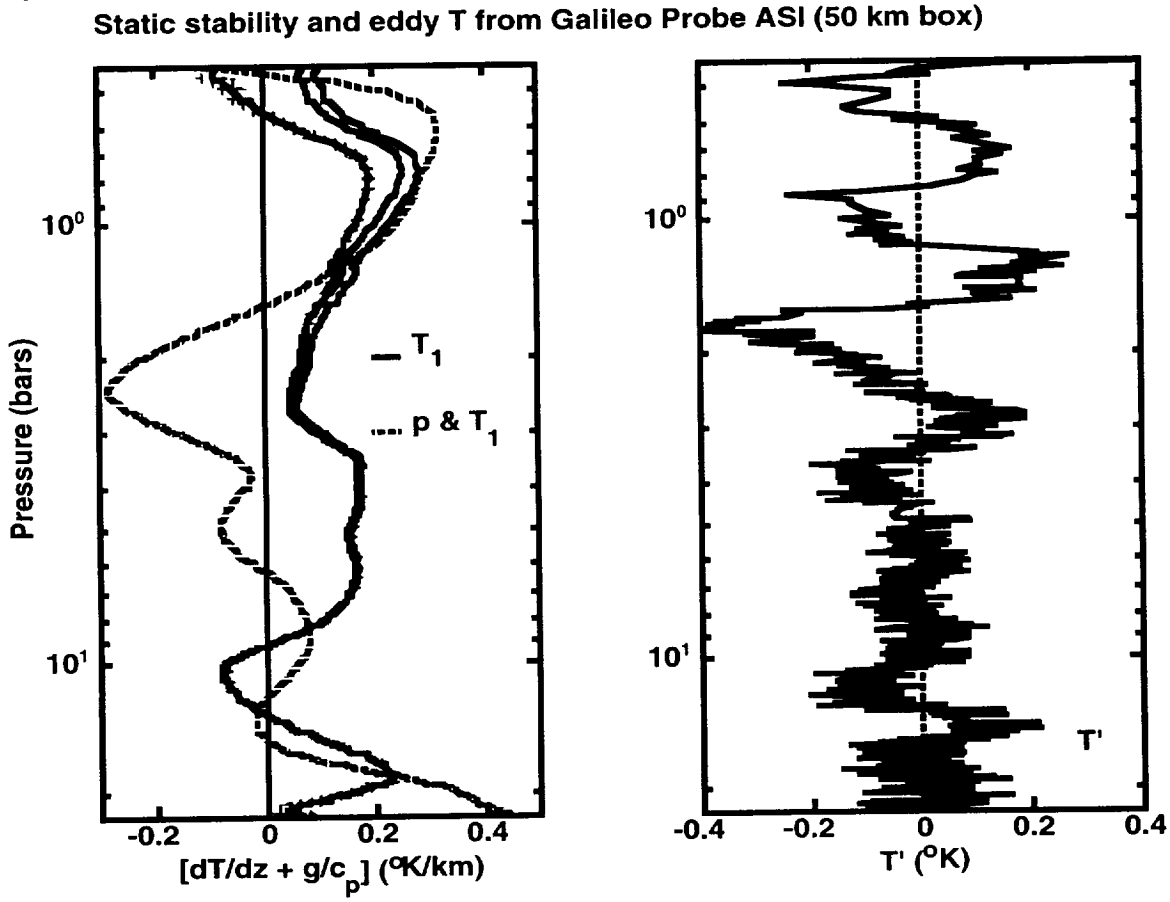

The presence of small scale atmospheric waves such as gravity waves that depend on static stability for their restoring force can also provide an indication of static stability. To isolate eddy structures

in the T measurements, we have subtracted the background values of T discussed above from the T measurements. This procedure is equivalent to applying a high spatial frequency-pass filter to the T observations. Figure 2b presents these results. Oscillatory structures with amplitudes of up to ~0.3°K and vertical wavelengths ~ 10-20 km are evident. T' with an amplitude that grows with height, as would be expected for a vertically propagating wave, is evident in the region (p< 10 bars), which shows positive background static stability. In addition, the observed apparent vertical wavelength agrees with the value expected for a gravity wave in an atmosphere with a constant static stability of 0.2°K/km and a plausible phase speed. Further work comparing the observed oscillations with the WKB theory of gravity waves is ongoing. The origin of the structure at p~ 12 bars is not yet understood, but it may be associated with presence of the region of static instability at p~ 10 bars.

Vertical gradients in the mean molecular weight can also contribute to the static stability of the atmosphere. For an unsaturated atmosphere with vertical gradients in molecular weight, a generalized expression for the static stability can be written as follows:

$$S=\left[\frac{dT}{dz}+\frac{g}{c_p}-\frac{T}{\bar{\mu}}\frac{d\bar{\mu}}{dz}\right] \quad (2)$$

where $\bar{\mu}$ is the mean molecular weight and other quantities have been previously defined. Figure 3a presents molecular weight versus pressure derived from the NMS measurements (Niemann et al, 1998) and from the NH_3 abundance retrieved by Folkner et al (1998) from absorption of the probe-orbiter radio signal. Figure 3b presents the contribution of the molecular weight gradient to the static stability. The vertical gradient in the molecular weight is governed by the vertical variation in the NH_3 abundance since the H_20 abundance and H_2S abundances were found to be low at the Galileo Probe PES. Note that at p<5 bars the NH_3 abundances are low and yield only a weak vertical gradient, while at p> 5 bars, significantly larger vertical gradients occur. At p~ 8 bars and at p~ 17 bars, the contribution to the static stability is ~ 0.1 K/km, which is of the right magnitude to stabilize the statically unstable region evident in fig. 2a at p~ 10 bars. However, the pressure levels of the peak contributions from the molecular weight term do not exactly match the pressure level of the observed static instability in the thermal profile. A possible explanation may be that the NH_3 abundance measurements pertain to the line-of-sight to the orbiter whereas the T sensor sampled temperature adjacent to the probe. Nevertheless, fig. 3b indicates that molecular weight gradients of the right magnitude and at approximately the right pressure levels exist and can make an important contribution to the static stability of Jupiter's atmosphere at the PES.

Figure 3a, b:

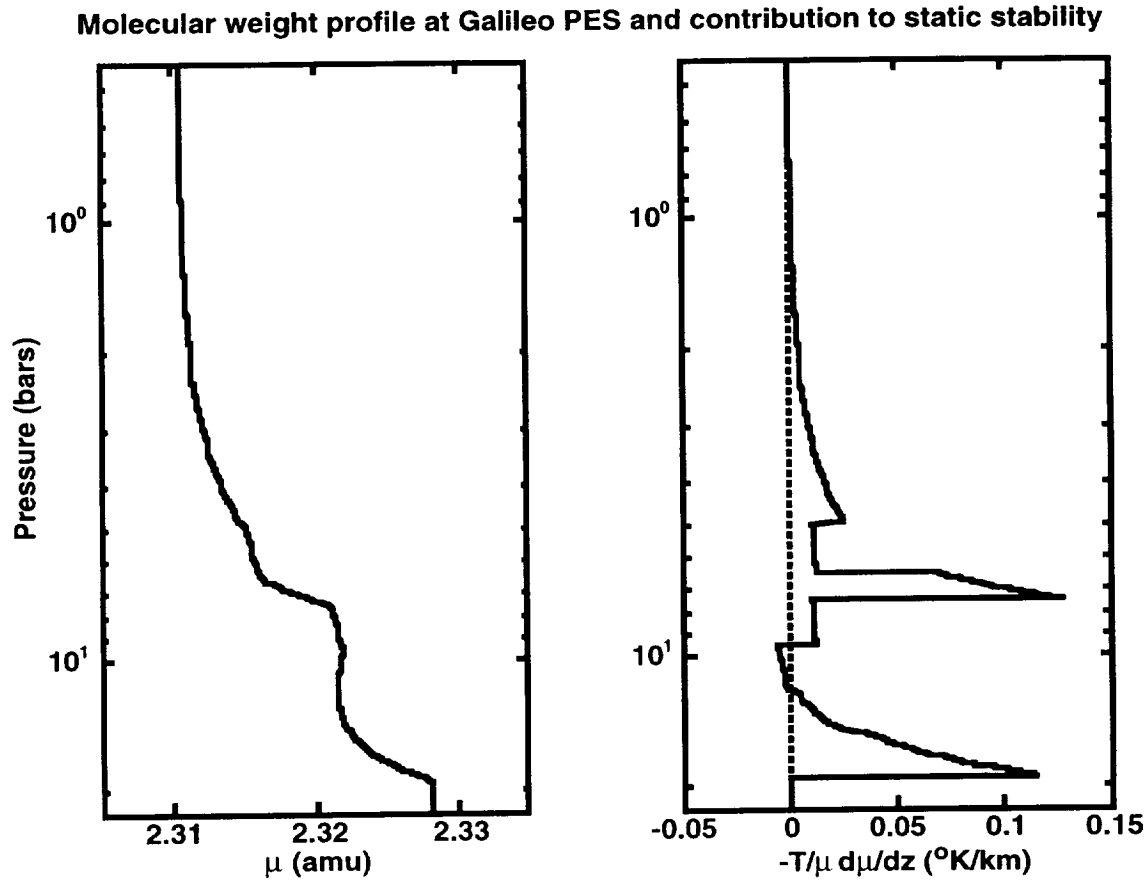

Atmospheric structure & dynamics evaluation using the Deep Space 2 Microprobes

Science Objectives:

Measurements of the deceleration history of an atmospheric entry probe can be used to derive the variation of atmospheric density, pressure, and temperature along the probe's trajectory through the atmosphere [Magalhães *et al.*, 1999, Seiff and Kirk, 1977]. Mars Microprobe Atmospheric Descent Accelerometer (ADA) data will be used to derive such atmospheric structure profiles along the trajectories of each of the microprobes from ~ 75 km altitude down to the surface. These data will provide the first atmospheric structure observations of the polar regions (~75° S latitude versus 19.1° N for Pathfinder, 22.3° N for Viking 1, and 47.6° N for Viking 2) and the first atmospheric structure measurements in the southern hemisphere. The Microprobes thus will provide a unique opportunity to investigate polar atmospheric structure and place observational constraints on the dynamics of the polar atmosphere. The late southern spring season (L_S=259°) of the entries will probe a quite different season than previous landers, which have all entered during northern summer, and thus will provide observational constraints on the dynamics at this season. The two Mars Microprobes, which will enter the martian atmosphere nearly simultaneously and

will impact the surface separated by a 10 km, will also provide the first opportunity to study the horizontal variability of local atmospheric structure over this length scale.

The relative contributions of different dynamical processes to the atmospheric circulation and structure of the polar regions is poorly constrained, and detailed observations of the thermal structure and water vapor distribution could provide useful information to constrain modeling efforts [Pollack *et al.*, 1990]. Understanding the dynamics of the polar regions is critical to assessing the water and dust cycles on Mars, since the dynamics govern the exchange of volatiles and dust between the polar regions and low latitudes [Jakosky and Haberle, 1992]. General circulation model results [Haberle *et al.*, 1993] suggest the microprobes will arrive in a region influenced by a circulation resulting from the temperature contrast between the cold residual cap and the warm surrounding terrain, analogous to a sea-breeze circulation. In addition, at the season of arrival, atmospheric dust levels will likely be increasing from the background levels studied during previous atmospheric entries and the atmospheric pressure will be near its annual maximum [Zurek *et al.*, 1992].

Due to the *in situ* nature of the measurement and the resulting high spatial resolution, the atmospheric structure profiles from the Mars Microprobes will provide unique information on atmospheric processes with vertical and horizontal scales smaller than 10 km. Atmospheric waves such as gravity waves with wavelengths in this range can be identified. Such waves can directly perturb the thermal structure and circulation and can also indirectly influence the atmosphere through the momentum and energy they transport vertically and meridionally [Barnes, 1990]. Convection and turbulence associated with unstable or neutral temperature lapse rates is potentially detectable. Atmospheric layers that are saturated with respect to carbon dioxide and water vapor can be identified and potentially associated with cloud or fog formation. The effects of aerosol layers (dust and condensates) also are potentially detectable in the temperature profile through their influence on direct solar heating and radiative cooling [Haberle *et al.*, 1999]. Thus, the observations from the ADA provide a valuable opportunity to make *in situ* measurements of atmospheric structure in the polar regions over a broad altitude range and to study the role of small-scale atmospheric processes in the polar atmosphere.

Instrument Description:
The ADA is mounted in the aftbody of the microprobe and is aligned parallel to the entry vehicle's axis of symmetry (z-axis) at a radial distance from the z-axis of about 25 mm. The ADA measures acceleration parallel to the z-axis only. The Mars Microprobe Atmospheric Descent Accelerometer is an Analog Devices ADXL250aqc unit. This device senses acceleration by measuring the capacitance between fixed plates and moveable plates that are elastically attached to the substrate of the device. Under the influence of an applied acceleration, the moveable plates are displaced until the elastic force balances the applied acceleration. The change in the plate position and hence the capacitance provides a measure of the applied acceleration. All of the circuitry needed to drive the

sensor and convert the capacitance change into an output voltage is included in the 5 gram highly integrated circuit of this surface micromachined device. The accelerometer has a range of -25 to 25 Earth g's. Output voltage from the ADA is digitized to 11 bits by an application specific integrated circuit (ASIC) to yield a digital resolution of 38 mg's / count (here mg's refers to milligravity units). Sampling and storage of data from the ADA is controlled by the telecommunication system of the microprobe. Data from the probes will be sampled at approximately 20 Hz, starting approximately 60 s before atmospheric entry and ending at impact.

The ADXL250 is an off-the-shelf microaccelerometer that has been used in a wide range of civilian and military applications including automobile airbags and howitzer shells. The manufacturer, Analog Devices, has extensively studied the performance of the units and compiled statistics on their characteristics based on testing of a large fraction of the units that have been assembled and shipped. Test results from the manufacturer span the temperature range -40° C to + 85° C, which includes the nominal expected probe temperature prior to atmospheric entry (-36°C) and the expected small internal heating associated with the atmospheric entry. Noise levels of a few mg's in the 0-100 Hz frequency range are well below the digital resolution of the experiment. The manufacturer's statistics show a spread of up to ±3% (1 standard deviation) in the scale factor of the units. Scale factor drift of 0.01% per °C and zero offset drift of 5 mg per °C is indicated by the data as well. Nonlinearity is typically ~0.2% of full scale. A flight spare unit has been tested and its characteristics are consistent with the manufacturer's specifications. Unfortunately, no calibration data for the flight units was acquired; however, as we discuss below, independent observations of the surface atmospheric density and the altitude of the probe impact site will provide a tight constraint on the scale factor of the flight units. Calibration data on the flight unit ASIC's define the transfer function of the analog-to-digital converter for the ADA. The relative timing between the ADA measurements is controlled by the telecommunications system's oscillator frequency whose drift with temperature has been measured.

Experiment Description:

Atmospheric density ρ is related to the aerodynamic deceleration of a spacecraft through the aerodynamic drag equation:

$$\rho = -\frac{2\,m}{C_D A}\,\frac{a_{vr}}{V_r^2} \quad (3)$$

where a_v is the acceleration along the flight path relative to the atmosphere, V_R is the probe velocity relative to the atmosphere, m is the probe mass, C_D is the drag coefficient of the probe, and A is the probe's cross-sectional area. The drag coefficient C_D varies during the entry, and this variation can be accounted for iteratively using aerodynamic databases compiled from pre-flight experiments and numerical simulations. For the Mars Microprobes $m/C_DA \sim 38$ kg m^{-2}. The velocity and position are derived by integrating over time the equations of motion of the vehicle using the measured

aerodynamic deceleration and knowledge of the gravity field [Magalhães *et al.*, 1999]. Trajectory solutions for the approach of the Mars Microprobes to Mars will be generated by the Mars Surveyor Navigation Team and will provide an initial condition for the trajectory integration. Atmospheric pressure versus altitude is derived by integrating the density profile using the equation of hydrostatic equilibrium. The ideal gas law along with a model for the molecular weight variation in the martian atmosphere then is used to derive atmospheric temperatures.

As can be seen from eq.(1), deceleration along the flight path is needed to derive the atmospheric structure, but the ADA measures acceleration along the z-axis only. The microprobes will enter the atmosphere at an unknown angle of attack (angle between velocity vector and z-axis of the probe) with unknown angular rate 30°/s. The aeroshell shape and mass distribution have been chosen so that aerodynamic torques in the upper atmosphere will reorient the vehicle to a small angle of attack by the time of peak deceleration and peak aerothermodynamic heating at 40-50 km altitude. Figure 4 presents the acceleration along the z-axis from a six-degree-of-freedom simulation of the Mars Microprobe entry by Braun *et al.* [1999]. Such simulations (note the ripple in Figure 4) and the theory of the angular motions of an entry vehicle show that the angle of attack oscillates about zero with decreasing amplitude and increasing frequency as the dynamic pressure, which is proportional to the atmospheric density, increases. Analytical expressions for the form of the oscillations derived from the simulations and the theory will be used to invert the z-axis acceleration measurements and derive the total angle of attack and deceleration along the flight path as a function of time.

For m/C_DA appropriate for the microprobes, the entry velocity of ~7 km/s, and the 38 mg digital resolution, eq. (1) indicates the ADA will begin sensing the atmosphere at $\rho \sim 5 \times 10^{-7}$ kg m^{-3}. Based on the Viking and Pathfinder entry profiles with a correction for the annual surface pressure variation of the Martian atmosphere, the threshold density corresponds to atmospheric detection at an altitude of about 90 km and to 10 counts at 75 km altitude. The vertical resolution of the profiles based on the vertical velocity of the microprobe, the angle of attack oscillation frequency, and the sampling frequency should vary between ~1 km at the start of the profile to ~100 meters as the surface is approached. The total probe accelerations after the deceleration peak in Figure 4 remain well above the acceleration of gravity until impact with the surface. Therefore, this indicates the probe continues decelerating due to atmospheric drag and does not achieve a balance between aerodynamic drag and the force of gravity (equilibrium descent) prior to impact. Since the microprobe remains within its aeroshell until impact, the Mars Microprobes will for the first time permit the use of accelerometer data to reconstruct atmospheric structure down to the surface of Mars. Previous landers have required pressure and temperature sensors to evaluate atmospheric structure below about 8 km during their parachute descent phases [Seiff and Kirk, 1977].

Probe velocity and flight path angle below horizontal (angle between velocity vector of probe and the local horizontal) from the entry simulations of Braun *et al.* [1999] are displayed in Figure 5.

Note that the impact velocity is predicted to be between 160-200 m/s and is strongly affected by the altitude of the impact site. The large velocities throughout entry, descent, and impact are well above predicted atmospheric winds so that the atmospheric structure analysis is relatively insensitive to the effects of winds. The flight path angle for an impact at 1 km altitude is ~80 degrees, resulting in an incidence angle of ~ 10 degrees for a level surface. Throughout most of the entry, the flight path angle is well below 80 degrees so that significant horizontal motion of the probe occurs during the traverse of the atmosphere.

Uncertainties in the atmospheric structure profiles will be governed by different factors during the course of the entry. Two key concerns are the uncertainty in the absolute time at which ADA observations are made and the value of the scale factor of the accelerometers. The relationship between spacecraft clock time and Universal Time is unknown to within 50 seconds due to uncertainty in the time required for the battery voltage to reach its nominal value and due to the lack of tiepoints between the spacecraft clock and events for which an absolute time is known. As a result, an unknown offset is introduced between the start time of the deceleration history measured by the ADA and the known absolute time of the initial entry velocity provided by the Mars Surveyor Navigation Team. This uncertainty significantly affects the position (altitude, latitude, longitude) assigned to the measurements thoroughout the entry and has a noticeable effect on the derived atmospheric density, pressure, and temperature after the deceleration peak (below ~ 40-50 km). The scale factor uncertainty has a monotonically increasing and strong effect on the error in the density, pressure, and temperatures after the deceleration peak (below ~ 40 km). Physically this strong effect after the decleration peak is due to the large decrease in velocity which controls the relationship between measured deceleration and derived density as shown in eq. (1).

Figure 6 illustrates the sensitivity of the impact altitude, surface atmospheric density, and impact velocity to uncertainties in the absolute time and the scale factor. These results were generated by introducing errors in absolute time and scale factor into the reconstruction of a deceleration history generated from an entry simulation through a known atmosphere. The strong sensitivity of the derived surface density and impact velocity to the scale factor error and the relatively weak dependance on the timing uncertainty indicates that an independent measurement of the surface atmospheric density or impact velocity provides a means of accurately determining the scale factor of the flight unit accelerometers.We will use measurements of the surface atmospheric density from the Mars Polar Lander's Meteorology experiment [Crisp *et al.*, 1999] to accurately determine the scale factors of the ADA's and thus to significantly increase the accuracy of the atmospheric structure profiles below ~ 40 km altitude. Determination of the landing site altitude by Doppler tracking of the radio signal from the Mars Microprobes will then be used to accurately determine the relationship between spacecraft clock time and Universal Time. This determination will permit accurate altitudes to be assigned to the measurements and will allow further refinement of the atmospheric structure profiles.

Additional uncertainties in the analysis include the angular alignment of the ADA with the z-axis, uncertainty due to the digital resolution, uncertainty in the aerodynamic properties of the microprobes, and uncertainties in the temperature dependence of the ADA and associated electronics. Any error in the alignment will be indistinguishable from error in the scale factor of the accelerometer; the procedure described earlier to solve for the scale factor will account for errors in the ADA alignment as well. Digitization uncertainty will be minimized by filtering the ADA observations with a low frequency-pass filter, which will effectively occur when we solve for the angle of attack and deceleration history, as described earlier. By applying the atmospheric structure profile reconstruction procedure to digitized and low-pass filtered deceleration histories computed from entry simulations into the atmospheric structure found by Viking 1, we find that all the major structures observed by Viking 1 in the middle and lower atmosphere could be observed with the microprobe measurements. Aerodynamic drag coefficient uncertainties [Mitcheltree *et al.*, 1999] introduce 1-3% error in the atmospheric density and pressure depending on the flight regime; uncertainty in the temperature is smaller and depends on the timescale over which the drag coefficient varies. ADA data will be collected prior to atmospheric detection, and this data will provide a good measure of the zero-g bias level of the ADA, thus facilitating detection of the atmosphere. The internal temperature of the microprobes is expected to be reasonably constant during the entry, descent, and impact phase (EDI) so that the variation with temperature of the characteristics of the ADA and associated electronics should be small, accountable via a linear temperature dependence, and should lead to only a small contribution to the uncertainties in the final result.

Relationship to Mars Polar Lander and other missions

The close proximity of the Mars Microprobe impact sites to the landing site of the Mars Polar Lander offers a unique opportunity for a coordinated investigation of the atmosphere. On-board accelerometers on the Mars Polar Lander will measure the deceleration of the lander to determine the timing of the start of the parachute descent phase. A small subset of this data will apparently be stored and returned to Earth although the suitability of this data for an investigation of atmospheric structure is unclear. Nevertheless, the returned data from the Mars Microprobes will offer higher vertical resolution and will enable derivation of atmospheric structure below the Mars Polar Lander's parachute release altitude of ~ 7 km. The Meteorology Experiment on the Mars Polar Lander will characterize the surface meteorology by measuring near-surface atmospheric temperatures, atmospheric pressure, winds, and humidity (Crisp et al, 1999). The atmospheric temperature profiles derived from the Mars Microprobe ADA experiment will allow an extension of the Mars Polar Lander observations of near-surface temperature and pressure to ~ 75 km altitude at two near-by locations.

The atmospheric light-detection and ranging (LIDAR) experiment on the Polar Lander will determine the altitude of dust hazes and ice clouds above the landing site within the lowest few kilometers (Linkin et al, 1999). The signature of dust and cloud opacity is potentially visible in

the atmospheric temperature profiles as heating due to increased absorption of sunlight by dust or enhanced radiative cooling produced by cloud opacity. In addition, by neglecting horizontal variability between the landing sites, the atmospheric structure profiles from the ADA can potentially provide information on the atmospheric temperatures associated with clouds or fogs observed by the LIDAR. As a result, determination of the saturation temperature of clouds and fogs and hence the water mixing ratios associated with the clouds may be possible. Therefore, the atmospheric science measurements from the Mars Polar Lander and from the Mars Microprobes provide highly complementary information which can yield valuable constraints on processes in the polar atmosphere of Mars.

The Mars Microprobe atmospheric structure profiles will also uniquely complement remote sensing observations of atmospheric temperatures from the Mars Global Surveyor (MGS) orbiter and the Mars Climate Orbiter (MCO). The better than 1 km vertical and horizontal resolution of the atmospheric structure profiles from the ADA provide the only means of characterizing atmospheric phenomena with vertical and horizontal scales smaller than 10 km. The Thermal Emission Spectrometer (TES) on MGS (Christensen et al, 1998) and the Pressure Modulator Infrared Radiometer (PMIRR) on the MCO (McCleese et al, 1992) will provide regional and global determinations of temperature on larger than 10 km horizontal scales and 5-10 km vertical scales. Observations of the Mars Polar Lander and Mars Microprobe landing areas near the time of the probe entries would be particularly valuable. Such measurements will allow the temperature profiles from the microprobes to be placed in a regional and seasonal context. In particular, horizontal variability between the Mars Polar Lander and Microprobe sites can be assessed and considered when comparing atmospheric measurements from these three probes.

Results on atmospheric structure and dynamics from the Pathfinder mission:
We report on a thorough analysis of the Mars Pathfinder Atmospheric Structure Investigation (ASI) accelerometer data spanning the altitude range 161 km - 8.9 km. Entry, descent, and landing occurred within 850 km of the Viking 1 lander and somewhat later in northern summer. The early morning entry (3 AM) provided the first opportunity to study Mars' nighttime atmospheric structure; the close proximity to the Viking 1 site has permitted a search for changes in atmospheric structure during the 21 years between the landings. Our results confirm and refine the major features of the atmospheric structure discovered in the initial analysis of the ASI results reported in Schofield et al (1997). The current analysis has yielded a much better definition of the temperature structure above 90 km altitude. Pathfinder measured a thermospheric peak temperature of 153°K at 134 km, which is 30°K colder than the value found by Viking 1. Between 110-88 km Pathfinder found a broad nearly isothermal plateau at 127°K, which correlates very well with a similar structure evident in Viking 1 data at the same pressures although the Pathfinder layer is 25°K colder. At levels above 88 km , wave-like oscillations with a wavelength ~5 km and amplitudes of 2-3°K are evident, possibly reflecting gravity or planetary wave activity. Between 90 km and 60 km the average temperature is 20-30°K cooler than Viking 1 values. Large amplitude

(10-20°K) long wavelength (20-40 km) oscillations, which show a remarkable correspondance to equivalent structures found in the Viking 1 profile at the same pressures, occur in this region and are likely due to a diurnal tidal mode. Between 85-77 km, a minimum of one oscillation results in temperatures up to 7°K below the saturation temperature of CO_2, well outside the uncertainties in the measurements and the vapor pressure curve and comparable to observed supersaturations of water in Earth's mesosphere. Between 55 km and 16 km, temperatures are close to or warmer than Viking 1 values; superposed long wavelength oscillations correspond well with similar structures observed by Viking 1. Between 16 km and 9.9 km, the temperature profile shows an unexpected strong thermal inversion, which may reflect radiative cooling due to a water cloud. At the base of the inversion, temperatures begin to increase abruptly until the last measurement at 8.9 km. The Viking-like temperatures in the lower atmosphere are consistent with the Viking-like dust optical depths observed by the Mars Pathfinder imager. The cool temperatures in the middle and upper atmosphere may be indicative of significant nighttime cooling at these levels although other interpretations are possible.

References:

Barnes, J.R., Possible effects of breaking gravity waves on the circulation of the middle atmosphere of Mars, *J. Geophys. Res.*, 95, 1401-1421, 1990.

Braun, R.D, R.A. Mitcheltree, F. M. Cheatwood, Mars microprobe entry analysis, *Journal of Spacecraft & Rockets* , 36, 1999.

Christensen, P.R., D.L. Anderson, S.C. Chase, R.T. Clancy, R.N. Clark, B.J. Conrath, H.H. Kieffer, R.O. Kuzmin, M.C. Malin, J.C. Pearl, T.L. Roush, M.D. Smith, Science 279, 1692-1698, 1998.

Crisp, D., A. Harri, R. May, G. R. Wilson, S. E. Wood, L. A. Leshin, R. Alleruzzo, C. LaBaw, C. Mahoney, R. Vargas Jr., O. E. Serviss, H. Gundersen, A. Lehto, J. Polku, I. J. McEwan, M. I. Richardson, R. W. Denise, R. W. Zurek, C. Hansen, D. A. Paige, The Meteorology instrument for the Mars Polar Lander Mars Volatile and Climate Surveyor payload, J. Geophys. Res., this issue., 1999.

Flasar, F.M. and P.J. Gierasch (1986). Mesoscale waves as a probe of Jupiter's deep atmosphere. *J. Atmos. Sci.* **43**, 2683-2707.

Folkner, W.M., R. Woo, and S. Nandi (1998). Ammonia abundance in Jupiter's atmosphere derived from the attenuation of the Galileo probe's radio signal. *J. Geophys. Res.* **103**, 22847-22855.

Haberle, R.M. *et al* , General circulation model simulations of the Mars Pathfinder atmospheric structure investigation/ meteorology data. *J. Geophys. Res.*, in press, 1999.

Haberle, R.M., J.B. Pollack, J.R. Barnes, R.W. Zurek, C.B. Leovy, J.R. Murphy, H. Lee, and J. Schaeffer, Mars atmospheric dynamics as simulated by the NASA Ames general circulation model 1. The zonal-mean circulation, *J. Geophys. Res., 98*, 3093-3123, 1993.

Jakosky, B.M. and R.M. Haberle, The Seasonal Behavior of Water on Mars, *Mars*, pp. 969-1016, The University of Arizona, Tucson, 1992.

Linkin,S. and S. Lipatov, The LIDAR experiment on the Mars Polar Lander, J. Geophys. Res., this issue, 1999

Magalhães, J.A., J.T. Schofield, and A. Seiff, Results of the Mars Pathfinder Atmospheric Structure Investigation, *J. Geophys. Res.*, in press, 1999.

McCleese, D. J., Haskins, R. D., Schofield, J. T., Zurek, R. W., Leovy, C. B., Paige, D. A., and Taylor, F. W. , Atmosphere and climate studies of Mars using the Mars Observer Pressure Modulator Infrared Radiometer. *J. Geophys. Res. 97(E5)*, 7735--7758, 1992.

Mitcheltree, R.A., J.N. Moss, F.M. Cheatwood, F.A. Greene, R.D. Braun, Aerodynamics of the

Mars Microprobe entry vehicles, AIAA paper 97-3658, August 1997.
Niemann, H.B., S.K. Atreya, G.R. Carignan, T.M. Donahue, J.A. Haberman, D.N. Harpold, R.E. Hartle, D.M. Hunten, W.T. Kasprzak, P.R. Mahaffy, T.C. Owen, and S.H. Way (1998). The composition of the Jovian atmosphere as determined by the Galileo probe mass spectrometer. *J. Geophys. Res.* **103**, 22831-22845.
Ortiz, J.L., G.S. Orton, A.J. Friedson, S.T. Stewart, B.M. Fisher, and J.R. Spencer (1998). Evolution and persistence of 5-μm hot spots at the Galileo probe entry latitude. *J. Geophys. Res.* **103**, 23051-23069.
Pollack, J.B., R.M. Haberle, J. Schaeffer, and H. Lee, Simulations of the general circulation of the Martian atmosphere, I. Polar processes, *J. Geophys. Res.*, 95, 1447-1474, 1990.
Seiff, A. and D.B. Kirk, Structure of the Atmosphere of Mars in Summer at Mid-Latitudes, *J. Geophys. Res.* 82, 4364-4378, 1977.
A. Seiff, D.B. Kirk, T.C.D. Knight, R.E. Young, J.D. Mihalov, L.A. Young, F.S. Milos, G. Schubert, R.C. Blanchard, and D. Atkinson (1998). Thermal structure of Jupiter's atmosphere near the edge of a 5-μm hot spot in the north equatorial belt. *J. Geophys. Res.* **103**, 22857-22889.
Smith, M.D. and P.J. Gierasch (1995). Convection in the outer planet atmospheres including ortho-para hydrogen conversion. *Icarus* **116**, 159-179.
Zurek, R. W. *et al.*, Dynamics of the Atmosphere of Mars. *Mars*, pp. 835-933. The University of Arizona, Tucson, 1992.

FIGURE 4. Aerodynamic deceleration along the z-axis of the Mars Microprobe from entry simulation by Braun et al [1999]. The digital resolution of the ADA and the surface acceleration of gravity have been plotted for comparison as well.

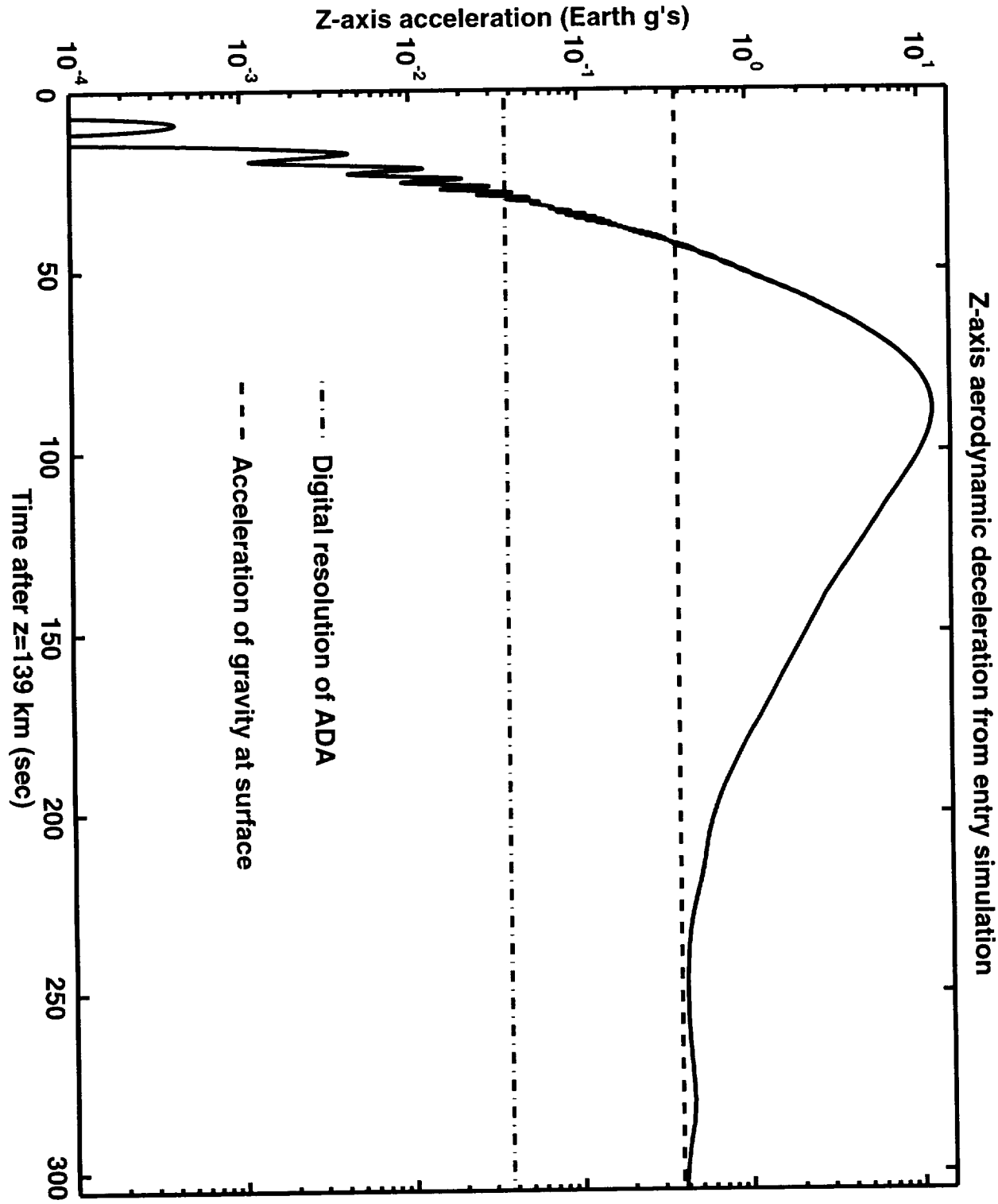

FIGURE 5. Probe velocity and flight path angle below horizontal from entry simulations by Braun et al [1999]. Flight path angle below horizontal is the angle between the velocity vector of the probe and the local horizontal.

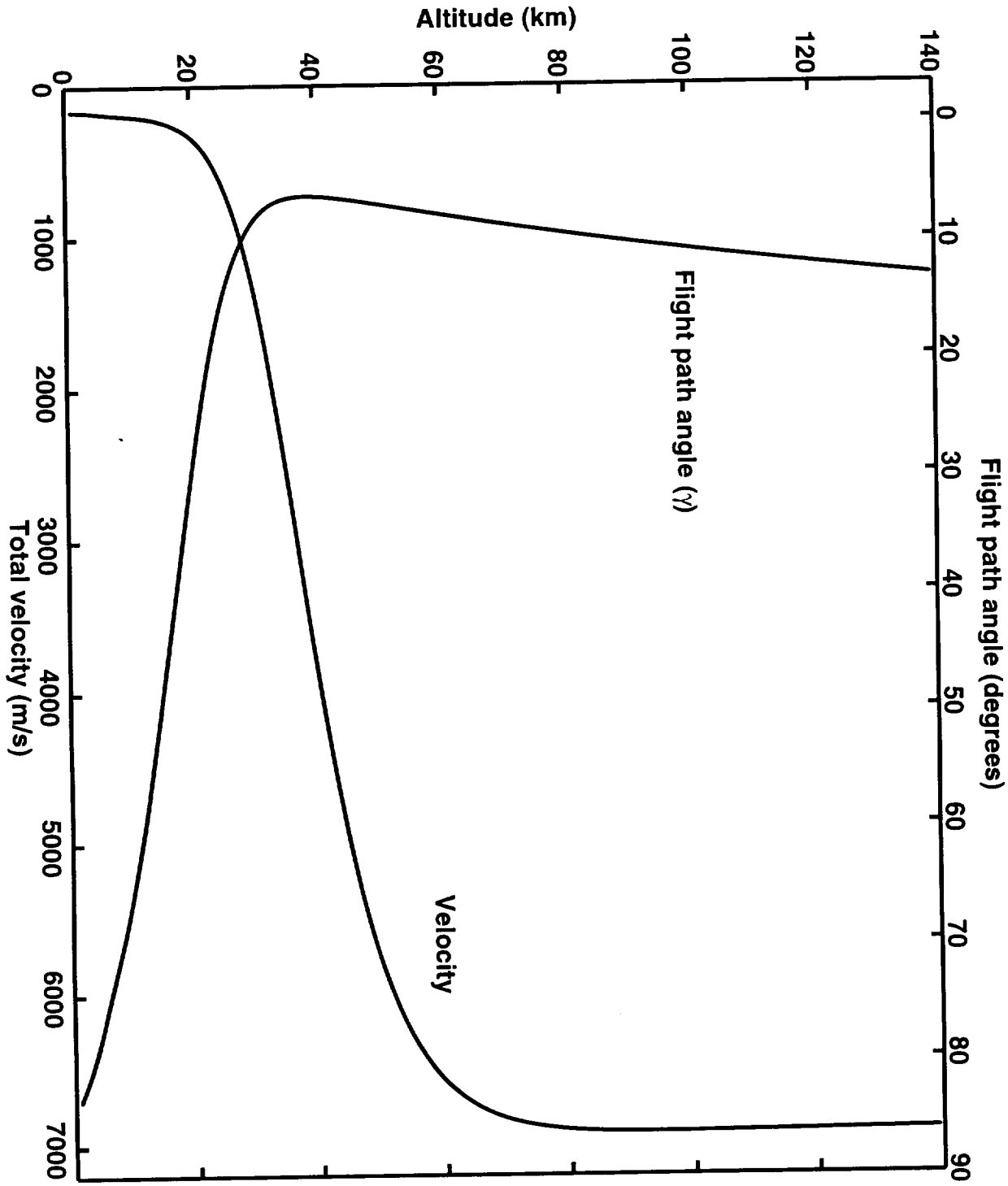

FIGURE 6. Effects of descent accelerometer scale factor error and absolute time error on quantities derived from atmospheric descent deceleration measurements. Derived impact altitude error, surface density error, and impact velocity error are plotted as functions of the error in the accelerometer's scale factor. In each subplot the errors are plotted for three values of the offset between spacecraft clock time and true Universal Time. $\Delta t = 0$ seconds corresponds to assigning the correct Universal Time (UT) to the zero of the spacecraft clock and hence to assigning the correct initial entry velocity to the trajectory integration. Similarly, $\Delta t = +3$ seconds corresponds to assigning spacecraft clock time to a UT that is 3 seconds later than the true UT. Note the strong dependance of the derived surface density and impact velocity on the scale factor error and the relatively weak dependance of these derived quantities on the absolute time errors. Independent determinations of the surface atmospheric density and/or impact velocity thus provide a powerful means of refining our knowledge of the descent accelerometer's scale factor. Independent determination of the impact altitude can then be used to derive the correct relationship between spacecraft clock time and Universal Time. Thus, measurement of the surface atmospheric density by the Mars Polar Lander MET experiment and determination of the impact locations by Doppler tracking of DS-2's radio signal will provide a powerful basis for increasing the accuracy of the atmospheric structure profiles.